2022 30th Mediterranean Conference on Control and Automation (MED)
June 28 - July 1, 2022. Athens, Greece

Model-Based/Model Predictive Control Design for Free Floating Space Manipulator Systems

Evangelos Psomiadis and Evangelos Papadopoulos, *Fellow, IEEE*

***Abstract*— The rapid increase in satellites and space debris mandates advanced capabilities for on-orbit operations. The hostile-to-human environment and the required high accuracy and robustness of on-orbit operations render Space Manipulator Systems (SMS) the appropriate choice. This work proposes an easily applicable, computationally inexpensive, nonlinear, and robust Cartesian control law for spatial Free-Floating SMS (FFSMS). The controller consists of two fundamental parts. The first is a Model-Based (MB) controller, which linearizes the system and guarantees prescribed performance. The second is a Model Predictive Controller (MPC), which integrates the model and provides optimal performance with parametric uncertainty, noise, and disturbances compensation. Input and output constraints are integrated into the latter to improve its performance. Numerical simulations for a planar model using Matlab/Simulink and MSC Adams highlight the MB/MPC's increased accuracy in comparison to a regular MB/PID controller, during a task that requires moving a captured object in the presence of parametric uncertainty, disturbances, and sensor noise. Monte-Carlo simulations substantiate the higher accuracy achieved by the MB/MPC.**

I. INTRODUCTION

On-orbit operations like assembling, capturing, refueling, repairing, and re-orbiting of satellites will become indispensable in the future. To cope with these tasks, national agencies and private companies have started investing in Space Manipulator Systems (SMS) already. Notable examples of such systems are the ETS-7 [1] and EU/ESA's under development EROSS+ [2] (see Figure 1).

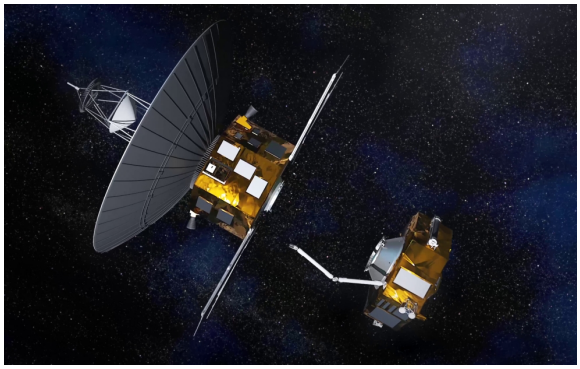

Figure 1. Picture of the EROSS+ vehicle and a target, [2].

An SMS consists of a satellite/base and one or more robotic manipulators. The base transfers and orients in space using its Attitude Determination and Control System (ADCS), which controls the momentum control devices such as the reaction wheels and thrusters. However, the motion of a manipulator's end-effector affects the base's motion and vice versa due to their dynamic coupling. The ADCS can be used to counterbalance this effect. Nonetheless, when the SMS is close to its target, the ADCS is turned-off to avoid undesirable disturbances from reaction wheels and thrusters, also minimizing fuel consumption. During this mode, only manipulator control systems operate, and the system is called a Free-Floating SMS (FFSMS).

In the past decades, many researchers have studied the dynamics and kinematics of an FFSMS [3], [4]. The concept of Dynamic Singularities (DS) that occur in an FFSMS due to the dependence of the end-effector's velocity to the manipulator and base's motion was introduced [5]. Umetani and Yoshida [6] presented the Generalized Jacobian Matrix for an FFSMS and a control method based on it.

Recent research focuses on studying FFSMS in more realistic conditions. Nanos and Papadopoulos extended the study of the dynamics and control of FFSMS in the presence of non-zero angular momentum [7] and flexible joint space manipulators [8]. Parametric uncertainty, disturbances, and sensor noise are also considered in the study of FFSMS. Parametric uncertainty might be caused by the variance of the base's mass due to fuel consumption or changes in the manipulator kinematics due to temperature variations. Robust control algorithms like an H_∞ Control [9] or a Model Predictive Control (MPC) can overcome such problems.

While MPC was initially used in slow systems such as chemical process industries [10], the evolution of computational hardware, as well as the MPC's simplicity and effectiveness in handling multi-variable and multi-constrained problems, permitted its application to faster systems. For example, Liao-McPherson et al. developed MPC laws for landing on an asteroid [11].

Notable studies have also been conducted in implementing MPC in SMS. Kayastha et al. presented a non-linear MPC to control the spacecraft's attitude and the end-effector's motion of a free-flying planar space manipulator with three links [12]. They compared their results with those from a Sliding Mode Control. Rybus et al. proposed a nonlinear MPC for FFSMS [13], [14]. They evaluated the controller by applying it to a planar FFSMS with a single two Degrees of Freedom (DoF) manipulator using a square reference end-effector trajectory and a capturing maneuver in the presence of disturbances and parametric uncertainty. MPC algorithms can be used in many space applications. However, the performance of a constrained MB/MPC in the

E. Psomiadis, and E. Papadopoulos are with the Department of Mechanical Engineering, National Technical University of Athens, Greece (e-mail: vaggelispsomiadis.02@gmail.com; egpapado@central.ntua.gr; phone: +30-210-772-1440).

presence of parametric uncertainty, disturbances, and sensor noise in a positioning task in orbit has not been studied so far.

In this paper, a Model-Based (MB) controller with an auxiliary MPC input is developed for spatial FFSMS; its performance is evaluated in the post-capture positioning of a satellite. This MPC is easier to apply than the controllers in [13] and [14]. The MB control law linearizes the system in an input-output sense to provide specific performance, while the MPC input integrates it and minimizes the errors from the desired trajectory, compensating for any disturbances. Input and output constraints are integrated into the design to improve the controller's performance. Numerical simulations show that the developed controller yields significantly smaller tracking error than an MB/PID controller in the presence of parametric uncertainty, disturbances, and sensor noise. The developed controller is simple, and its computational needs are almost the same to those of an MB/PID controller since most of the calculations are performed offline. The controller is developed for spatial Cartesian motions and is evaluated here with an example of a planar FFSMS equipped with a single 3 DoF manipulator.

II. Dynamics of FFSMS

The dynamics of a spatial FFSMS with a single manipulator of N DoF are described. Assuming a rigid manipulator, inactive base actuators, zero external forces and torques, and zero initial momentum, the conservation of angular momentum yields [7]

$$\mathbf{h}_{CM} = \mathbf{R}_0(\boldsymbol{\varepsilon},n)\left[{}^0\mathbf{D}(\mathbf{q}){}^0\boldsymbol{\omega}_0 + {}^0\mathbf{D}_q(\mathbf{q})\dot{\mathbf{q}}\right] = \mathbf{0}_{3x1} \quad (1)$$

where $\mathbf{R}_0$ is the rotation matrix between the base's frame and the inertial frame, expressed as a function of base's Euler parameters $\boldsymbol{\varepsilon}$ and n, ${}^0\boldsymbol{\omega}_0$ is the base's angular velocity expressed in the base's frame, ${}^0\mathbf{D}$, ${}^0\mathbf{D}_q$ are inertia-type matrices given in [3], $\mathbf{q}$ and $\dot{\mathbf{q}}$ are the joint angles, and angular velocities respectively and $\mathbf{0}_{3x1}$ is the 3x1 zero vector.

Solving (1) for ${}^0\boldsymbol{\omega}_0$ as a function of $\dot{\mathbf{q}}$, and substituting in the end-effector differential kinematics [7]:

$$\mathbf{v}_E = \begin{bmatrix} \dot{\mathbf{r}}_E \\ \boldsymbol{\omega}_E \end{bmatrix} = \begin{bmatrix} \mathbf{R}_0(\boldsymbol{\varepsilon},n) & \mathbf{0}_{3x3} \\ \mathbf{0}_{3x3} & \mathbf{R}_0(\boldsymbol{\varepsilon},n) \end{bmatrix} {}^0\mathbf{J}^*(\mathbf{q})\dot{\mathbf{q}} \quad (2)$$

where ${}^0\mathbf{J}^*$ is called the Generalized Jacobian Matrix [6] which is a function of the joint angles $\mathbf{q}$, and $\mathbf{0}_{3x3}$ is 3x3 zero matrix.

The end-effector's attitude can be expressed using Euler angles $\boldsymbol{\theta}_E$

$$\boldsymbol{\omega}_E = \mathbf{S}(\boldsymbol{\theta}_E)\dot{\boldsymbol{\theta}}_E \quad (3)$$

where $\mathbf{S}(\boldsymbol{\theta}_E)$ is a 3x3 matrix.

Substituting (3) into (2)

$$\dot{\mathbf{x}}_E = \begin{bmatrix} \dot{\mathbf{r}}_E & \dot{\boldsymbol{\theta}}_E \end{bmatrix}^T = \mathbf{J}\dot{\mathbf{q}} \quad (4)$$

where $\mathbf{x}_E$ is a 6x1 vector which contains the end-effector's positions and angles and $\mathbf{J}$ is the Jacobian matrix, given by

$$\mathbf{J} = \begin{bmatrix} \mathbf{I}_3 & \mathbf{0}_{3x3} \\ \mathbf{0}_{3x3} & \mathbf{S}^{-1}(\boldsymbol{\theta}_E) \end{bmatrix} \begin{bmatrix} \mathbf{R}_0(\boldsymbol{\varepsilon},n) & \mathbf{0}_{3x3} \\ \mathbf{0}_{3x3} & \mathbf{R}_0(\boldsymbol{\varepsilon},n) \end{bmatrix} {}^0\mathbf{J}^*(\mathbf{q}) \quad (5)$$

It is important to point out that $\mathbf{J}$ is also a function of dynamic properties such as masses and inertias. This characteristic results in the existence of dynamic singularities in addition to the kinematic ones [5]. Therefore, additional caution must be given during end-effector path planning.

Considering the above, the reduced equations of motion of a spatial FFSMS in the joint space are [4]

$$\mathbf{H}(\mathbf{q})\ddot{\mathbf{q}} + \mathbf{C}(\mathbf{q},\dot{\mathbf{q}})\dot{\mathbf{q}} = \boldsymbol{\tau} \quad (6)$$

where $\boldsymbol{\tau}$ contains the manipulator joint torques (dimensions Nx1), since the base actuators are inactive. $\mathbf{H}$ is the reduced system inertia matrix and $\mathbf{C}$ contains the nonlinear Coriolis and centrifugal terms, given by

$$\begin{aligned} \mathbf{H}(\mathbf{q}) &= {}^0\mathbf{D}_{qq} - {}^0\mathbf{D}_q^T {}^0\mathbf{D}^{-1} {}^0\mathbf{D}_q \\ \mathbf{C} &= \frac{1}{2}\frac{\partial\left(\dot{\mathbf{q}}^T {}^0\mathbf{D}_q^T {}^0\mathbf{D}^{-1} {}^0\mathbf{D}_q\right)}{\partial\mathbf{q}} + \frac{\partial\left({}^0\mathbf{D}_{qq}\dot{\mathbf{q}}\right)}{\partial\mathbf{q}} \\ &\quad - \frac{1}{2}\frac{\partial\left(\dot{\mathbf{q}}^T {}^0\mathbf{D}_{qq}\right)}{\partial\mathbf{q}} - \frac{\partial\left({}^0\mathbf{D}_q^T {}^0\mathbf{D}^{-1} {}^0\mathbf{D}_q\dot{\mathbf{q}}\right)}{\partial\mathbf{q}} \end{aligned} \quad (7)$$

with ${}^0\mathbf{D}_{qq}$ being an inertia-type matrices and is given in [3].

Differentiating (4) yields

$$\ddot{\mathbf{x}}_E = \mathbf{J}\ddot{\mathbf{q}} + \dot{\mathbf{J}}\dot{\mathbf{q}} \quad (8)$$

Solving (4) for $\dot{\mathbf{q}}$ and (8) for $\ddot{\mathbf{q}}$ and substituting them into (6) yields

$$\mathbf{H}_x\ddot{\mathbf{x}}_E + \mathbf{C}_x\dot{\mathbf{x}}_E = \mathbf{f} = \mathbf{J}^{-T}\boldsymbol{\tau} \quad (9)$$

where

$$\begin{aligned} \mathbf{H}_x &= \mathbf{J}^{-T}\mathbf{H}\mathbf{J}^{-1} \\ \mathbf{C}_x &= \mathbf{J}^{-T}\left(\mathbf{C} - \mathbf{H}\mathbf{J}^{-1}\dot{\mathbf{J}}\right)\mathbf{J}^{-1} \end{aligned} \quad (10)$$

Eq. (10) describes the equations of motion of a spatial FFSMS in Cartesian space and will be used for the implementation of the controller in the next section.

III. MB/MPC Design

A. Controller Design

The controller consists of two parts, see Figure 2. The first is an MB controller with PD action, which linearizes and decouples the FFSMS' dynamics and guarantees specific performance. The second is an MPC, which integrates the model and provides optimal performance with parametric uncertainty and disturbances compensation.

It is considered that the desired trajectories of end-effector position and orientation $\mathbf{x}_d(t)$, and their 1st and 2nd derivatives are defined, sensors are used for the joints' angles $\mathbf{q}$, angular velocities $\dot{\mathbf{q}}$, and the base's Euler parameters $\boldsymbol{\varepsilon}$ and n. The end-effector position and orientation $\mathbf{x}_E$, and their derivatives, are calculated too, and the matrices $\mathbf{H}_x$, $\mathbf{C}_x$ and $\mathbf{J}$ are calculated using (5), (7) and (10) for each time step but with a bounded error due to the parametric uncertainty (the symbol "^" denotes an estimate of "·"). Then, the MB controller is given by

$$\begin{aligned} \mathbf{f} &= \hat{\mathbf{H}}_x\left[\ddot{\mathbf{x}}_d + \mathbf{K}_D\dot{\mathbf{e}}_x + \mathbf{K}_P\mathbf{e}_x + \mathbf{u}_{MPC}\right] + \hat{\mathbf{C}}_x\dot{\mathbf{x}}_E \\ \boldsymbol{\tau} &= \hat{\mathbf{J}}^T\mathbf{f} \end{aligned} \quad (11)$$

where $\mathbf{K}_D$ and $\mathbf{K}_P$ are NxN gain matrices, $\mathbf{u}_{MPC}$ is the MPC input, which is discussed in detail in next subsection, and

$$\mathbf{e}_x = \left(\mathbf{x}_d - \mathbf{x}_E\right) \tag{12}$$

Substituting (11) into (9), the dynamics equations of the closed-loop system are

$$\begin{aligned} \ddot{\mathbf{e}}_x + \mathbf{K}_D\dot{\mathbf{e}}_x + \mathbf{K}_P\mathbf{e}_x &= \mathbf{d}_{unc} - \mathbf{u}_{MPC} \\ \mathbf{d}_{unc} &= \hat{\mathbf{H}}_x^{-1}\left(\left(\mathbf{H}_x - \hat{\mathbf{H}}_x\right)\ddot{\mathbf{x}}_E + \left(\mathbf{C}_x - \hat{\mathbf{C}}_x\right)\dot{\mathbf{x}}_E\right) \end{aligned} \tag{13}$$

where $\mathbf{d}_{unc}$ is the vector generated by the parametric uncertainty of the FFSMS. Considering that the vector $\mathbf{d}_{unc}$ is either zero or counterbalanced by the MPC action, (13) is a linearized and decoupled set of equations since the gain matrices $\mathbf{K}_D$ and $\mathbf{K}_P$ are diagonal.

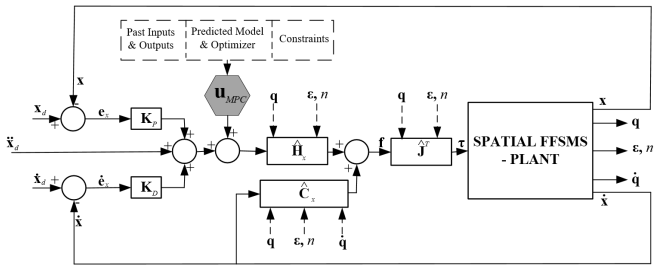

Figure 2. Block Diagram of the MB/MPC applied to a Spatial FFSMS in Cartesian Space

B. MPC Input

The term MPC can designate a plethora of advanced control methods which use a model for output prediction while minimizing an objective function and obtaining a control sequence. These also use a "receding horizon" according to which the final future time instant is consistently displaced forward and only the first instant's control signal is applied. Figure 2 depicts the controller in block diagram form.

The applied MPC algorithm is a state-space linear MPC [15]. By disregarding the disturbances for representation simplification and considering that after the application of the MB controller, the system is linearized and decoupled, the state-space model for each end-effector variable is

$$\begin{aligned} \dot{\mathbf{z}}_\mathbf{m}(t) &= \mathbf{A}_\mathbf{m}\mathbf{z}_\mathbf{m}(t) + \mathbf{B}_\mathbf{m}u_{MPC}(t) \\ y(t) &= \mathbf{C}_\mathbf{m}\mathbf{z}_\mathbf{m}(t) \end{aligned} \tag{14}$$

with

$$\begin{aligned} \mathbf{z}_\mathbf{m} &= \begin{bmatrix} z_{m,1} & z_{m,2} \end{bmatrix}^T = \begin{bmatrix} e_x & \dot{e}_x \end{bmatrix}^T, \\ \mathbf{A}_\mathbf{m} &= \begin{bmatrix} 0 & 1 \\ -K_P & -K_D \end{bmatrix}, \mathbf{B}_\mathbf{m} = \begin{bmatrix} 0 \\ -1 \end{bmatrix}, \mathbf{C}_\mathbf{m} = \begin{bmatrix} 1 & 0 \end{bmatrix} \end{aligned} \tag{15}$$

Orthonormal functions are used for the control signal's representation in continuous time. A prerequisite is that its variable's integral squared value must be bounded [16]. Therefore, the controller is designed using the derivative of the signal, and the system's augmented model is used

$$\begin{aligned} \dot{\mathbf{z}}(t) &= \mathbf{A}\mathbf{z}(t) + \mathbf{B}\dot{u}_{MPC}(t) \\ y(t) &= \mathbf{C}\mathbf{z}(t) \end{aligned} \tag{16}$$

with

$$\begin{aligned} \mathbf{z} &= \begin{bmatrix} \dot{z}_{m,1} & \dot{z}_{m,2} & y \end{bmatrix}^T \\ \mathbf{A} &= \begin{bmatrix} 0 & 1 & 0 \\ -K_P & -K_D & 0 \\ 1 & 0 & 0 \end{bmatrix}, \mathbf{B} = \begin{bmatrix} 0 \\ -1 \\ 0 \end{bmatrix}, \mathbf{C} = \begin{bmatrix} 0 \\ 0 \\ 1 \end{bmatrix}^T \end{aligned} \tag{17}$$

The orthonormal functions chosen are the Laguerre functions defined as

$$\mathbf{L}(t) = e^{\mathbf{A}_\mathbf{p}t}\mathbf{L}(0) \tag{18}$$

with

$$\mathbf{A}_\mathbf{p} = \begin{bmatrix} -p & 0 & \dots & 0 \\ -2p & -p & \dots & 0 \\ \vdots & \ddots & \ddots & \vdots \\ -2p & \dots & -2p & -p \end{bmatrix}, \ \mathbf{L}(0) = \sqrt{2p}\begin{bmatrix} 1 \\ 1 \\ \vdots \\ 1 \end{bmatrix} \tag{19}$$

where the parameter p is the time scaling factor and is a design requirement which determines the exponential decay rate of the set of functions. Using the above functions, the control signal is written as

$$\dot{u}_{MPC}(\tau) = \sum_{j=1}^{N_L} c_j l_j(t) = \mathbf{L}(\tau)^\mathrm{T}\boldsymbol{\eta}, \ 0 \le \tau \le T_p \tag{20}$$

where T_p is the prediction horizon, N_L is the number of the Laguerre functions employed, and $\boldsymbol{\eta} = [c_1\ c_2\ \dots\ c_N]^\mathrm{T}$ is the vector of coefficients which is an optimization process result.

The cost function used for the optimization is given by

$$\begin{aligned} J = \int_0^{T_p} &(\mathbf{z}(t+\tau\,|\,t)^T\mathbf{Q}\mathbf{z}(t+\tau\,|\,t) + \dot{\mathbf{u}}_{MPC}(\tau)^T\mathbf{R}\dot{\mathbf{u}}_{MPC}(\tau))d\tau \\ &0 \le \tau \le T_p \end{aligned} \tag{21}$$

where the matrices $\mathbf{Q}\ge 0$ and $\mathbf{R}\ge 0$ are weighting factors and can be used to tune the performance index fittingly.

It is shown that the cost function is minimized when [15]

$$\boldsymbol{\eta} = -\boldsymbol{\Omega}^{-1}\boldsymbol{\Psi}\mathbf{z}(t) \tag{22}$$

with

$$\begin{aligned} \boldsymbol{\Omega} &= \int_0^{T_p}\boldsymbol{\varphi}(\tau)\mathbf{Q}\boldsymbol{\varphi}(\tau)^\mathrm{T}d\tau + \mathbf{R}_\mathbf{L}, \\ \boldsymbol{\Psi} &= \int_0^{T_p}\boldsymbol{\varphi}(\tau)\mathbf{Q}e^{\mathbf{A}\tau}d\tau, \ 0 \le \tau \le T_p \end{aligned} \tag{23}$$

where τ is a time instant within the prediction time window and $\mathbf{R}_\mathrm{L}$ is a block diagonal matrix given by

$$\mathbf{R}_\mathbf{L} = diag\{r_k\mathbf{I}_{N_L\times N_L}\}, k = 1-6 \tag{24}$$

where r_k is the k diagonal element of $\mathbf{R}$ and $\mathbf{I}_{\mathrm{NLxNL}}$ is the identity matrix of dimensions N_LxN_L.

The vector $\boldsymbol{\varphi}$ results from the prediction of the plant response and it is calculated numerically by solving

$$\mathbf{A}\boldsymbol{\varphi}(\tau)^T - \boldsymbol{\varphi}(\tau)^T\mathbf{A}_\mathbf{p}^T = -\mathbf{B}\mathbf{L}(\tau)^T + e^{\mathbf{A}\tau}\mathbf{B}\mathbf{L}(0)^T \tag{25}$$

To satisfy the principle of the receding horizon control that only the control signal at $\tau=0$ is to be considered, and that the prediction horizon "moves", the control input of the augmented model is given by

$$\dot{\mathbf{u}}_{MPC}(t) = \mathbf{L}(0)^T\boldsymbol{\eta} = -\mathbf{L}(0)^T\boldsymbol{\Omega}^{-1}\boldsymbol{\Psi}\begin{bmatrix} \dot{\mathbf{z}}_\mathbf{m}(t) \\ \mathbf{y}(t) - \mathbf{y}_d(t) \end{bmatrix} \tag{26}$$

Therefore, the control signal of the initial model is given by integrating the above equation, also proving the integral action of the MPC

$$\mathbf{u}_{MPC}(t) = \int_0^t \dot{\mathbf{u}}_{MPC}(\gamma)\, d\gamma \tag{27}$$

C. MPC Constraints

The MPC has the advantage of easy introduction of input or output constraints, regardless of the time instant at which they occur, or the duration of the constraints. To insert the constraints into the design, they must be written in the form

$$\mathbf{A}_{constr}\boldsymbol{\eta} \le \mathbf{b} \tag{28}$$

The vector $\boldsymbol{\eta}$ is then calculated using Hildreth's quadratic programming procedure [17]. By setting an upper and lower limit for the control signal, the following inequalities apply

$$\mathbf{u}_{\min} \le \mathbf{u}_{MPC}(t) \le \mathbf{u}_{\max} \tag{29}$$

Hence, the input constraints on the amplitude of the control signal are given by

$$\begin{bmatrix} \Delta t\mathbf{L}(0)^T \\ -\Delta t\mathbf{L}(0)^T \end{bmatrix}\boldsymbol{\eta} \le \begin{bmatrix} \mathbf{u}_{\max} - \mathbf{u}_{MPC}(t_i - \Delta t) \\ -(\mathbf{u}_{\min} - \mathbf{u}_{MPC}(t_i - \Delta t)) \end{bmatrix} \tag{30}$$

Similarly, the output constraints are given by

$$\begin{bmatrix} \mathbf{bL}(0)^T \\ -\mathbf{bL}(0)^T \end{bmatrix}\boldsymbol{\eta} \le \begin{bmatrix} \dot{\mathbf{z}}_{\max} - \mathbf{A}\mathbf{z}_{\max} \\ -(\dot{\mathbf{z}}_{\min} - \mathbf{A}\mathbf{z}_{\min}) \end{bmatrix} \tag{31}$$

IV. Example & Results

In this section, an example is employed to illustrate the performance of the proposed controller. Without loss of generality, a planar FFSMS with a single 3 DoF manipulator is used for the post-capture motion of a satellite in Cartesian space. In the first simulation, the parameters of the manipulator and the captured object are not accurately known but estimated. Constant disturbances are inserted into the simulation. Figure 3 shows the kinematic structure and parameters of the FFSMS with the captured target, while Table I presents the nominal parameter values and the disturbances.

The second simulation includes sensor noise in addition to all the above. For the last simulation, the parameters of the FFSMS vary between known bounds, and a Monte-Carlo simulation is performed. All the results are compared to the performance of an MB/PID controller.

The captured object is regarded as part of the 3rd link. The mass of the composite 3rd link and captured object is

$$m_3' = m_3 + m_s \tag{32}$$

while the inertia is given by

$$I_3' = I_3 + I_s + m_3\left(l_3' - l_3\right)^2 + m_s r_3'^2 \tag{33}$$

where m_s and I_s are the mass and the inertia of the captured object respectively, l_3' is the distance between the 3rd joint and the new CM, r_3' is the distance between the new CM and the CM of the captured object and they are given by

$$l_3' = \frac{m_3 l_3 + m_s\left(l_3 + r_s\right)}{m_3 + m_s},\ r_3' = r_s + l_3 - l_3' \tag{34}$$

where r_s is the distance between the CM of the 3rd link and the CM of the captured object.

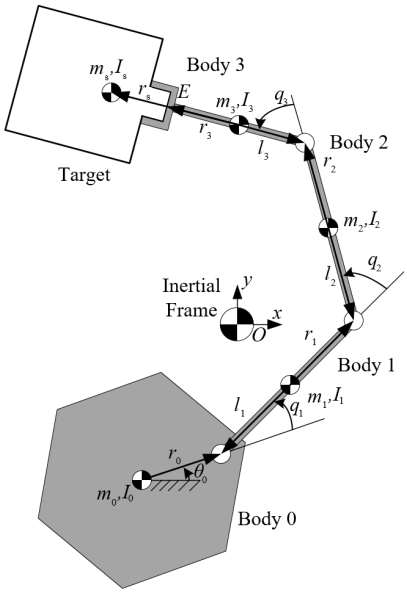

Figure 3. Planar FFSMS with a Single Manipulator with 3 DoF.

Table I. FFSMS & Captured Object's Parameters

Parameter	Base	1st Link/ Joint	2nd Link/ Joint	3rd Link/ Joint	Captured Object
m (kg)	600	40	40	20	200
I (kgm^2)	500	20	20	15	100
$r + l$ (m)	1.4	1 + 1	1 + 1	0.25 + 0.25	0.8
Disturb. (Nm)	-	12	6	4	-

In both simulations, the end-effector is commanded to move from point (0.5556 m, 1.8542 m) with orientation 95° to point (-0.25 m, 1.5 m) with orientation 120° . No dynamic singularities are encountered. The duration of the simulation is 6 s. Figure 4 includes snapshots of the motion of the FFSMS in the ADAMS environment for three different time instants (with orange is the FFSMS). The white line depicts the trajectory of the end-effector.

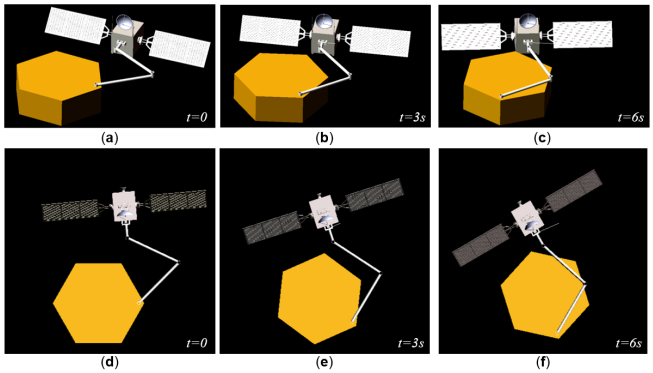

Figure 4. Snapshots of the Motion of the FFSMS in the ADAMS environment for three different time-points and two different views (a) Isometric View (t=0), (b) Isometric View (t=3s), (c) Isometric View (t=6s), (d) Top View (t=0), (e) Top View (t=3s), (c) Top View (t=6s).

To apply the MB/MPC controller, its gains and parameters must be determined. To reduce the risk for overshoots and impacts, the damping ratio is taken as $\zeta = 1$. To keep the maximum applied torques reasonable, the natural frequency is chosen as $\omega_n = 1$ rad/s. Considering the above as the prescribed desired performance of the FFSMS, the controller gains are computed as

$$K_D = diag(2,2,2), K_P = diag(1,1,1) \tag{35}$$

The scaling factor of Laguerre functions is set equal to the dominant pole of the respective LQR problem [15] i.e., $p = 5.0167$ rad/s. Parameters N_L and T_p are determined through several trials to achieve values above which the results of the simulations remain immutable. Consequently, $N_L = 10$ and $T_p = 6$ s. Finally, matrix $\mathbf{Q}$ is set equal to the transpose of the matrix of the output, multiplied by the matrix of the output, and $\mathbf{R}$ is set adequately small since the goal of the controller is to lessen the error and not the input signal

$$\mathbf{Q} = \mathbf{C}^T\mathbf{C} = \begin{bmatrix} 0 & 0 & 0 \\ 0 & 0 & 0 \\ 0 & 0 & 1 \end{bmatrix}, \mathbf{R} = 10^{-6} \tag{36}$$

To be compared with the developed controller, an MB/PID controller is employed, given by

$$\mathbf{f} = \hat{\mathbf{H}}_x\left[\ddot{\mathbf{x}}_d + \mathbf{K}_D{}'\dot{\mathbf{e}}_x + \mathbf{K}_P{}'\mathbf{e}_x + \mathbf{K}_I{}'\int_0^t \mathbf{e}_x(\lambda)d\lambda\right] + \hat{\mathbf{C}}_x\dot{\mathbf{x}}_E \tag{37}$$

$$\boldsymbol{\tau} = \hat{\mathbf{J}}^T\mathbf{f}$$

Setting the ζ and ω_n equal to the ones selected for the MB/MPC and using the characteristic equation

$$\begin{aligned} &s^3 + K_{D,i}{}'s^2 + K_{P,i}{}'s + K_{I,i}{}' = \\ &\left(s+\omega_n\right)\left(s^2 + 2\zeta\omega_n s + \omega_n^2\right),\ i = 1,2,3 \end{aligned} \tag{38}$$

the MB/PID controller's gains are computed as

$$\begin{aligned} &\mathbf{K}_D{}' = diag(3,3,3), \mathbf{K}_P{}' = diag(3,3,3), \\ &\mathbf{K}_I{}' = diag(1,1,1) \end{aligned} \tag{39}$$

Case 1: For the 1st simulation, the target and the base mass manifest a 10% parametric uncertainty, while all the other parameters have 5%. To achieve a partial convergence of the errors at the steady-state, constraints were integrated on the MB/MPC. In particular, the constraints were inserted after the time-step $t=5s$ and until the end of the simulation. These output/error constraints are

$$\mathbf{z}_{\max} = \begin{bmatrix} 4\cdot10^{-5} & 5\cdot10^{-6} & 3.5\cdot10^{-4}\pi/180 \end{bmatrix}^T = -\mathbf{z}_{\min} \tag{40}$$

However, because the output constraints contain the risk of torque surge, input constraints on the MPC signal u_{MPC} defined in (27) are also introduced. So, if the signal exceeds these values, they become active

$$\mathbf{u}_{\max} = \begin{bmatrix} 0.05 & 0.05 & 0.05 \end{bmatrix}^T = -\mathbf{u}_{\min} \tag{41}$$

Figure 5(a) presents the errors of the x-coordinate, the y-coordinate, and the orientation of the end-effector. Figure 5(b) shows the torques $\boldsymbol{\tau}$ of the manipulator given by (11), and (37). It is obvious that the MB/MPC has better results than the MB/PID controller in all three variables without requiring additional control effort. In particular, the MB/MPC achieves a 100% reduction of all the variables while the maximum torques exhibit a difference of 3% which can be considered negligible.

Considering that the calculations are performed offline for non-active constraints and that when constraints are active, Hildreth's Quadratic programming procedure is converged in 1-2 loops, the computational power that both controllers require is almost identical. For example, by performing ample simulations in Matlab/Simulink on the same computer, the duration was about 90 s for both designs.

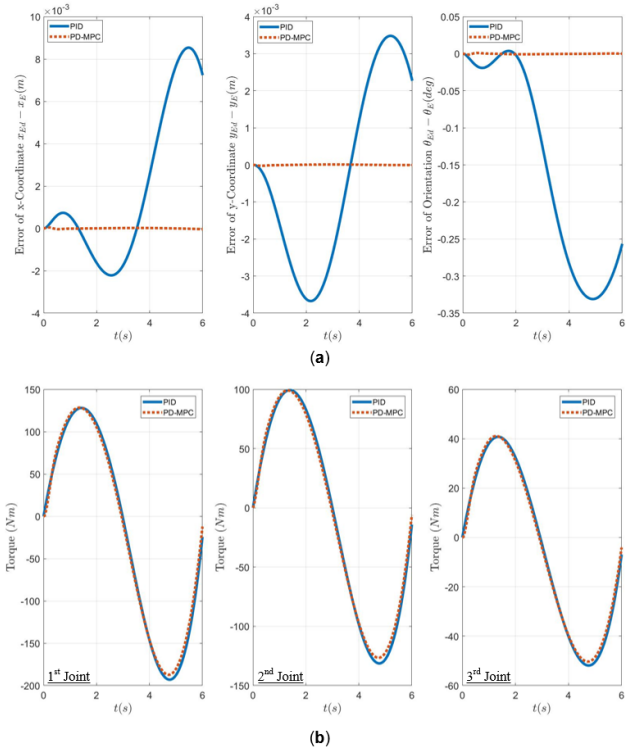

Figure 5. (a) Error of the Actual and the Desired Value of the Joints' Angles (b) Torques of the Manipulator's Joints.

Case 2: The 2nd simulation does not include constraints, but noise is introduced in joint angles, base's attitude, end-effector's variables, and all their derivatives. The noise is considered normally distributed with a zero mean and variance $\sigma^2 = 10^{-8}$ (where σ is the standard deviation). Figure 6 displays the errors of the end-effector's x-coordinate, y-coordinate, and orientation.

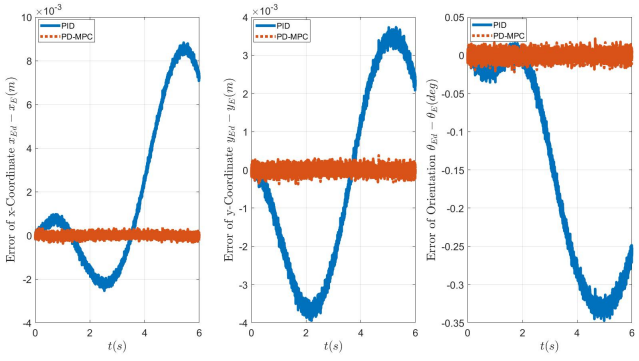

Figure 6. Error of the Actual and the Desired Value of the Joints' Angles for normally distributed zero-mean noise with variance $\sigma^2 = 10^{-8}$.

It is concluded that the MB/MPC compensates for Gaussian noise with $\sigma^2 = 10^{-8}$ successfully. However, if the process variables contain higher variance noise, the compared controllers manifest similar behavior.

Case 3: Finally, Monte-Carlo simulations were performed to validate the controller's performance when parametric uncertainties and disturbances are present. The nominal values of the FFSMS and the target, as well as the disturbances are given in Table I. These parameters vary to cover a wide range of uncertainty. The variation is based on (Base:0, Links:1-3, Target:4)

$$\begin{aligned} 0.95l_{i,nominal} \le l_i \le 1.05l_{i,nominal} \quad & i=0,...,4 \\ 0.95r_{i,nominal} \le r_i \le 1.05r_{i,nominal} \quad & i=0,...,4 \\ 0.95m_{i,nominal} \le m_i \le 1.05m_{i,nominal} \quad & i=1,...,3 \\ 0.90m_{0,nominal} \le m_0 \le 1.05m_{0,nominal} & \\ 0.90m_{4,nominal} \le m_4 \le 1.10m_{4,nominal} & \end{aligned} \tag{42}$$

The results of the 200 simulations performed for both controllers are displayed in Figure 7. The errors of the position and orientation of the end-effector are shown. The MB/MPC significantly improves the results by reducing the error by two orders of magnitude, while, due to its design, it needs almost the same computational power.

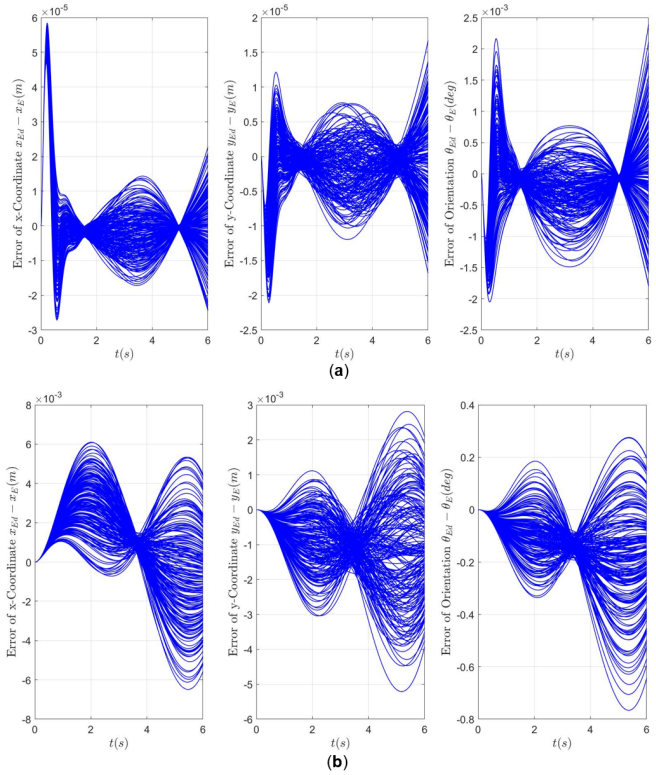

Figure 7. Tracking error using Monte-Carlo Simulation for the 200 Different Random Samples (a) MB/MPC, (b) MB/PID.

V. Conclusion

In this paper, an MB/MPC is developed for an FFSMS during on-orbit operations in 3D Cartesian space. The MB part linearizes the system and provides specific performance, while the MPC part minimizes the tracking errors and compensates for disturbances. Input and output constraints are integrated into the MPC for improved performance. A planar example of an FFSMS with a 3 DoF manipulator positioning a satellite, demonstrates that the MB/MPC yields significantly smaller tracking errors than an MB/PID controller in the presence of parametric uncertainty, disturbances, and sensor noise. The MB/MPC is simple, and its computational needs are almost the same to those of the MB/PID controller since most of the computations are performed offline. Three illustrative cases were presented to corroborate this position. In the future, further comparisons will be tried, especially with nonlinear robust controllers.

References

[1] Oda, M., "Space robot experiments on NASDA's ETS-VII satellite preliminary overview of the experiment results," *Proceedings 1999 IEEE International Conference on Robotics and Automation*, Detroit, MI, USA, May 10-15, 1999. DOI: 10.1109/ROBOT.1999.772555.

[2] https://eross-h2020.eu/eross-plus/.

[3] Papadopoulos, E., and Dubowsky, S., "Coordinated Manipulator/Spacecraft Motion Control for Space Robotic Systems," *IEEE International Conference on Robotics and Automation (ICRA '91)*, Vol. 2, April 9-11, 1991, Sacramento, CA, pp.1696-1701.

[4] Papadopoulos, E., and Dubowsky, S., "On the Nature of Control Algorithms for Free-Floating Space Manipulators," *IEEE Transactions on Robotics and Automation*, Vol. 7, No.6, December 1991, pp. 750-758.

[5] Papadopoulos, E., and Dubowsky, S., "Dynamic Singularities of Free-Floating Space Manipulators," *ASME Journal of Dynamic Systems, Measurement, and Control*, Vol. 115, No. 1, March 1993, pp. 44-52.

[6] Umetani, Y., and Yoshida, K., "Resolved Motion Rate Control of Space Manipulators with Generalized Jacobian Matrix," *IEEE Transactions on Robotics and Automation*, Vol. 5, No. 3, June 1989, pp. 303-314.

[7] Nanos, K. and Papadopoulos, E., "On the Dynamics and Control of Free-floating Space Manipulator Systems in the Presence of Angular Momentum," *Frontiers: Robotics & AI - Space Robotics*, June 29, 2017. DOI: 10.3389/frobt.2017.00026.

[8] Nanos, K. and Papadopoulos, E., "On the Dynamics and Control of Flexible Joint Space Manipulators," *Control Engineering Practice*, Vol. 45, December 2015, pp. 230-243.

[9] Taveira, T., Siqueira, A., and Terra, M., "Adaptive Nonlinear H_∞ Controllers Applied to a Free-Floating Space Manipulator," *IEEE International Conference on Control Applications*, Munich, Germany, October 4-6, 2006, pp. 1476 - 1481.

[10] Garcia, C.E., Prett, D.M., and Morari, M., "Model Predictive Control: Theory and Practice-a Survey," *Automatica*, 25(3), May 1989, pp. 335–348.

[11] Liao-McPherson, D., Dunham, W., and Kolmanovsky, I.V., "Model Predictive Control Strategies for Constrained Soft Landing on an Asteroid," *Proceedings of AIAA/AAS Astrodynamics Specialist Conference*, Long Beach, California, AIAA Paper 2016-5507, DOI: 10.2514/6.2016-5507, 2016.

[12] Kayastha S., Shi, L., Katupitiya, J., and Pearce, G., "Nonlinear model predictive control of a planar three-link space manipulator," *11th Asian Control Conference (ASCC)*, Gold Coast, QLD, Australia, December 17-20 2017. DOI: 10.1109/ASCC.2017.8287244.

[13] Rybus T., Seweryn K., and Sasiadek J.Z. "Control System for Free-Floating Space Manipulator Based on Nonlinear Model Predictive Control (NMPC)," *Journal of Intelligent and Robotic Systems 85*, 2017, pp. 491-509.

[14] Rybus T., Seweryn K., and Sasiadek J. Z., "Nonlinear Model Predictive Control (NMPC) for Free-Floating Space Manipulator," *Aerospace Robotics III. GeoPlanet: Earth and Planetary Sciences*. Springer, November 2018, pp. 17-29.

[15] Wang, L., *Model Predictive Control System Design and Implementation Using MATLAB*, Springer-Verlag, London, UK, 2009.

[16] Lee, Y. W., *Statistical Theory of Communication*, John Wiley and Sons, New York, 1960.

[17] Hildreth, C., "A quadratic programming procedure," *Naval Research Logistics Quarterly*, 4(1), pp. 79–85. DOI: 10.1002/nav.3800040113.